10 YEARS ANNIVERSARY

INORGANIC
CHEMISTRY

FRONTIERS

RESEARCH ARTICLE

Check for updates

Crystal growth of the 2D Janus rhodium chalcohalide RhSeCl†

Domenic Nowak, [ID] *[a] Martin Valldor, [ID] [b] Bastian Rubrecht, [ID] [a,c] Samuel Froeschke, [ID] [a] Samar Eltoukhy,[a] Bernd Büchner, [ID] [a,c] Silke Hampel [ID] *[a] and Nico Gräßler [ID] *[a]

The rapidly growing interest in synthesising 2D Janus materials is supported by the numerous theoretical predictions of the unique properties of this material category. Here, we report the discovery of the novel 2D Janus material RhSeCl, which crystallises in a space group with a hexagonal symmetry, $P6_3mc$, with the unit cell parameters a = 3.48760(10) and c = 11.5791(5) Å. Crystals of RhSeCl exhibit a plate-like morphology, which is typical of 2D materials. We present two methods of synthesising RhSeCl, either as polycrystalline powder *via* a solid-state reaction or as single crystals *via* chemical vapour transport, the latter allowing the control of the crystal size and thickness. Using XRD, SEM and EDX, we show that the described method has high reproducibility. The direct deposition of the 2D Janus crystal RhSeCl provides a broader approach to the study of the Janus phenomena and could further be adjusted to other promising element combinations.

1 Introduction

Functional solid-state materials, and in particular, inorganic oxides, halides and chalcogenide compounds, have a wide range of applications.[1] Specific examples include the use of $LiMn_2O_4$ as a cathode material in Li-ion batteries, $TiCl_3$ as a catalyst for the polymerisation of olefins[2,3] and MoS_2 as a semiconductor in transistors.[4,5] Further development of these compounds is mainly focused on the variation of cations, whereas the influence of anions, particularly the combination of different anions, is seldom investigated. These so-called "mixed anion compounds" or "heteroanionic materials" represent a new type of artificial inorganic material with unique, distorted coordination geometries and, thus, crystal structures. Accordingly, the combination of two anions opens up a whole new level in material design and should lead to compounds with chemical and physical novelties.[1,6]

Two-dimensional (2D) Janus materials represent a unique family among mixed anionic compounds. In Janus compounds, different atoms are positioned on either side of an atomic layer, breaking the mirror symmetry.[7–9] The term "Janus" is derived from the two-faced Roman god and was introduced by Casagrande in 1989.[10] Theoretical studies have shown that the broken symmetry leads to new physical, chemical and quantum phenomena, *e.g.* Rashba splitting[11] and vertical piezoelectricity, making them good candidates for the use in skyrmions/ quantum optospintronics.[12] The Janus concept represents a novel form of functionalisation, and the interest in these materials is growing rapidly. So far, only a few representatives of 2D Janus materials have been reported, for example, graphene-based Janus-layers,[13] Janus transition metal dichalcogenides such as MoSSe[14] and 2D Janus chalcohalides such as BiTeCl.[11,15] However, there is a large gap between the theoretical predictions and the experimental results, which is probably related to the difficulties in sample preparation.[7–9] The search for novel materials with the Janus structure and the optimisation for simple synthesis strategies therefore are important steps towards the development of this category of materials.

Here, we present the novel 2D Janus material RhSeCl synthesised by a solid-state reaction (SSR) and chemical vapour transport (CVT). The latter is a scalable method that allows us to control both the film thickness and the size of the crystals. Depending on the parameters, single crystals of size as large as 0.2 millimeters are formed. The elemental uniformity of the polycrystalline powder and crystal structure is confirmed by a variety of characterisation techniques. Finally, our work allows an easily accessible synthesis of 2D Janus crystals and provides a broad access to study the phenomena of the Janus concept in detail.

[a]Leibniz-Institute for Solid State and Materials Research Dresden, Helmholtzstraße 20, D-01069 Dresden, Germany. E-mail: d.nowak@ifw-dresden.de, s.hampel@ifw-dresden, n.graessler@ifw-dresden.de
[b]Department of Chemistry, University of Oslo, NO-0315 Oslo, Norway
[c]Institute for Solid State Physics, Technical University Dresden, D-01062 Dresden, Germany
†Electronic supplementary information (ESI) available. See DOI: https://doi.org/10.1039/d2qi02699f

This journal is © the Partner Organisations 2023

Inorg. Chem. Front., 2023, **10**, 2911–2916 | **2911**

2 Results and discussion

2.1 Synthesis process

The preparation of polycrystalline samples of RhSeCl *via* a one-step solid-state reaction of Se and $RhCl_3$ was first postulated by Kretschmer.[16] A drawback of this synthesis method is the formation of $SeCl_4$ or Se_2Cl_2 during the synthesis. To circumvent the involvement of these impurities, elemental rhodium was included in the reaction (see ESI Fig. S1†). A gray-black powder was obtained and small crystals precipitate on the ampoule wall. The quality of the polycrystalline sample was investigated with powder X-ray diffraction. The XRD patterns did not indicate any additional impurities and the Rietveld refinement (see Fig. 1) confirmed an excellent fit to the proposed structure model (see also section 3).

As small crystals and significant recrystallisation were observed from the solid-state reaction, an approach to synthesise 2D Janus crystals of RhSeCl *via* CVT was optimised. For the initial crystal growth, the parameters reported by Köhler *et al.*[17] for the endothermic transport of RhTeCl were adapted: $\Delta T = 200$ K ($T_1 = 700$ °C, $T_2 = 900$ °C, and 72 h).[18] Instead of elemental chlorine, rhodium(III) chloride was used as a chlor-

ine source. However, it turned out that the selected thermal gradient was too large, as the crystals only deposited in the middle area of the ampoule. By reducing the temperature gradient to 100 K (from 950 °C to 850 °C), smaller single crystals in the size range of 20–50 μm as well as polycrystals with a size of up to 150 μm were acquired. As shown in ESI Fig. S2† we have adapted the synthesis further in order to grow larger crystals. By increasing the transport time to 10 days, shifting the transport temperature from 1000 °C to 900 °C and adding a small excess of $RhCl_3$ as an additional transport agent, polycrystals with a size of about 1.8 mm were obtained. Further variation of the reaction time and a change in the stoichiometric amount of $RhCl_3$ showed small effects on the crystal size (see Fig. S2†).

2.2 Microscopy

Powder samples of RhSeCl are greyish-black, whereas single crystals grown by chemical vapour transport are black with a metallic lustre. The SEM image at higher magnification shows platelet-shaped crystallites with characteristic edge angles around 60° and 120° in a trigonal form, while layers show a hexagonal symmetry (see Fig. 2). Generally, the layered structure of the crystal with the hexagonal basic structure is recognisable with both light and scanning electron microscopes.

According to energy dispersive X-ray spectroscopy (EDX) analyses, the elemental composition of the crystallites agrees with the expected composition within the errors of EDX measurements. However, the strong overlap of the Cl and Rh X-ray emissions made the determination of these elements less reliable (see ESI Fig. S3†). The elemental analysis from an average of 5 area measurements indicates a composition close to $Rh_{35.6(3)}$ $Cl_{30.5(3)}$ $Se_{33.9(6)}$ (see ESI Table S1†). In addition the EDX-mapping shows a uniform distribution of the elements, as shown in Fig. 2.

2.3 Crystal structure

Single-crystal X-ray diffraction showed that RhSeCl crystallises in a hexagonal symmetry with the cell parameters $a = 3.48760$ (10) Å and $c = 11.5791(5)$ Å. From the observed reflection extinction conditions and intensity distributions, the polar and non-centrosymmetric space group $P6_3mc$ was assigned. The detailed results obtained from the structure refinement of rhodium selenide chloride are listed in Table 1, and the crystal structure is shown in Fig. 3. Each rhodium atom is co-
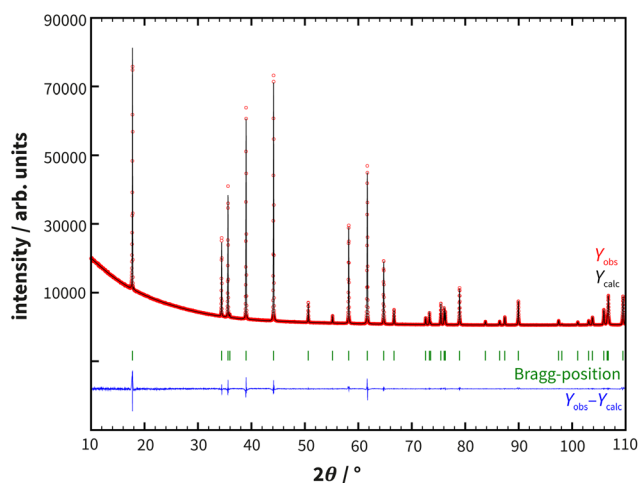
Fig. 1 Powder X-ray diffraction data of RhSeCl with superimposed Rietveld refinement simulations (see Table 1) and their corresponding differences. The measurement was carried out using a Co X-ray source ($\lambda = 1.78896$ Å).
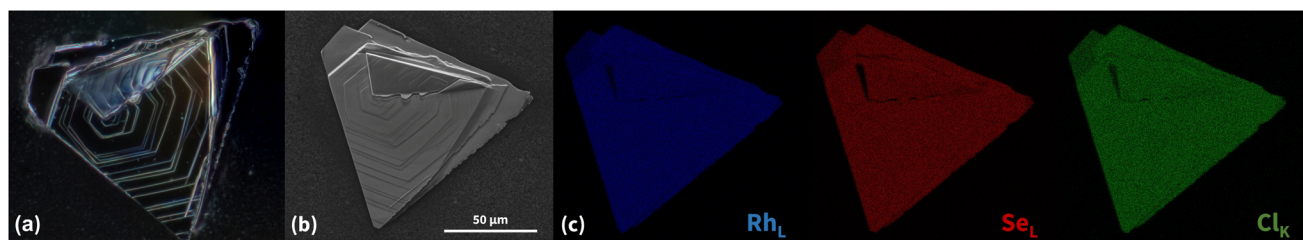
Fig. 2 (a) Microscopy image of a grown RhSeCl single crystal, with a hexagonal layered structure. (b) SEM image of the same crystal, with some edge effects. (c) EDX spectroscopy mapping of the main elements of the title compound, showing an even distribution of the elements.

2912 | *Inorg. Chem. Front.*, 2023, **10**, 2911–2916

This journal is © the Partner Organisations 2023

Table 1 Crystal structure parameters from a single crystal and Rietveld refinement of RhSeCl

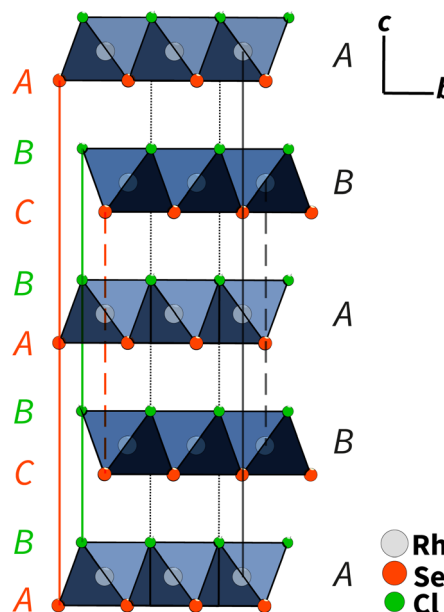| Measurement method	SC-XRD	PXRD
Empirical formula	RhSeCl	RhSeCl
Temperature (K)	293	293
Wavelength (Å)	0.71073 (MoK$_\alpha$)	1.78896 (CoK$_\alpha$)
Crystal system	Hexagonal	Hexagonal
Space group	$P6_3mc$	$P6_3mc$
Z	2	2
Unit cell dimensions (Å)	a = 3.48760(10)	a = 3.48982 (6)
	c = 11.5791(5)	c = 11.5889 (3)
Cell volume (Å^3)	V = 121.972(7)	V = 122.230 (4)
Density (calculated) (g cm^{-3})	5.9172	5.9047
Absorption coefficient (mm^{-3})	22.592	123.569
$F(000)$	192	192
Theta range for data collection	6.76 to 49.29°	10.00 to 110.71°
Index ranges	$-7 \leq h \leq 7$; $-7 \leq k \leq 7$; $-24 \leq l \leq 24$	
Reflections collected	7481	43
Independent reflections	545	
Constraints/restraints/ parameters	1/0/10	1/0/7
Goodness-of-fit on F^2	1.9	2.9
Final R indexes [$I \leq 2\sigma(I)$]	R_1 = 0.0358; wR_2 = 0.0861	R_1 = 0.0464; wR_2 = 0.0564
Final R indexes [all data]	R_1 = 0.0431; wR_2 = 0.0879	R_1 = 0.0464; wR_2 = 0.0564
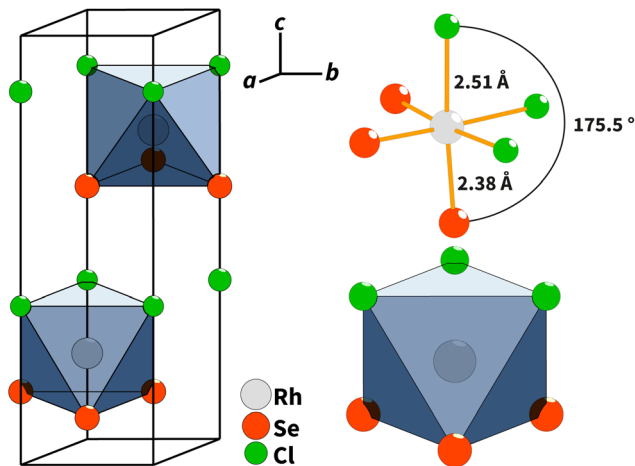
Fig. 3 (Left) Crystal structure of RhSeCl in the perspective view with an outlined unit cell. (Right) Facially heteroleptic coordination of Rh with the atomic distances and the coordination polyhedra.[20]

Fig. 4 AB type layer stacking of RhSeCl in the $c-b$ direction. The anions are ordered in an ABCBA sequence, where the selenium atoms have two different positions (layers) due to symmetry. One repetition from C to C for the selenium atoms corresponds to one full length of the unit cell in the c direction ($\approx$11.6 Å).[20]

ordinated by three Cl atoms with a distance of 2.5104(9) Å and three selenium atoms with a distance of 2.3829(8) Å in a facial arrangement, resulting in distorted octahedra. The non-metal atoms are coordinated to three rhodium atoms. Thereby, the edge-sharing Rh-octahedra form the basis for the individual layers. The individual layers in RhSeCl stack in an AB arrangement (see Fig. 4). The stacked layers are only weakly bonded by van der Waals interactions, which is a typical characteristic of 2D materials.[19] The anions arrange themselves according to

their type in opposite sides, forming the typical Janus structure. The individual anions are stacked in an ABCBA sequence (see Fig. 4) and one full repetition of that sequence is equivalent to the length of the c-axis. The height of a monolayer is 2.78 Å and the distance between two rhodium layers is 5.79 Å.

To highlight the effect of the mixed anions on the crystal structure, we compare them with structurally related single anion compounds. When looking at the bond lengths of the binary single anion compounds, rhodium(III) selenide[21] and rhodium(III) chloride,[22] in relation to the heteroanionic RhSeCl, a difference is obvious. The distance between rhodium and selenium is comparable for the chalcohalide and chalcogenide. On the other hand, the distance between rhodium and chlorine in RhSeCl is about 0.2 Å longer than that in RhCl$_3$, but equivalent to the corresponding interatomic distances in RhTeCl (see ESI Table S2†). The reason for this alteration of bond lengths could probably be the steric hindrance. It is noticeable that the octahedron height grows simultaneously with the incorporation of larger elements such as selenium or tellurium.

In contrast to RhTeCl, RhSeCl has the undistorted CdI$_2$ structure type. Furthermore, the two rhodium chalcohalides also differ in the type of edge linkage of the Rh-octahedra. In RhTeCl, the edges are linked either only *via* the tellurium or chlorine atoms, while in RhSeCl both chlorine and selenium are linked at the same edge of the octahedron.

According to the Neumann principles, RhSeCl, described being in the space group $P6_3mc$, should be both piezoelectric and pyroelectric,[23,24] which will be investigated in the near future. Furthermore, this material should have non-linear

This journal is © the Partner Organisations 2023

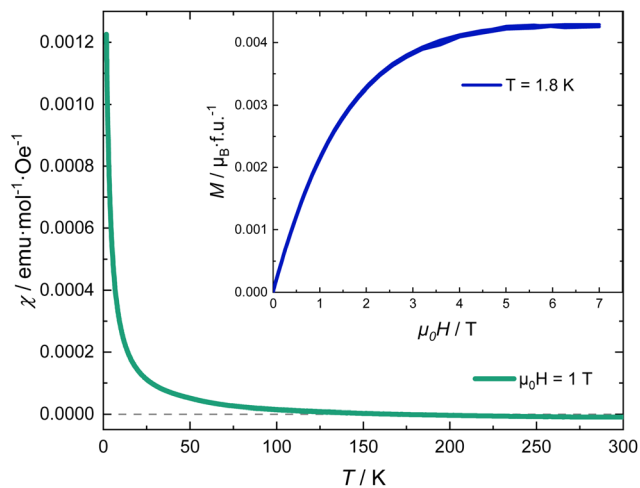*Inorg. Chem. Front.*, 2023, **10**, 2911–2916 | **2913**

Fig. 5 Magnetic susceptibility of a polycrystalline RhSeCl sample in the temperature range from 2 to 300 K measured with an applied field of $\mu_0 H = 1$ T. The inset shows the field dependence of the magnetisation per formula unit measured at $T = 1.8$ K.

optical properties,[25,26] such as second-harmonic-generation (SHG), but this optical property might be quenched due to the dark coloring of the compound.

2.4 Magnetic measurements

Fig. 5 shows the magnetic susceptibility of RhSeCl in the temperature range from 2 to 300 K. Above ~150 K, the curves show diamagnetic behaviour with a paramagnetic Curie-tail for the low-temperature regime. The inset in Fig. 5 shows the field dependence of the magnetisation measured at 1.8 K for applied fields up to 7 T. We observe a magnetic moment that saturates at $0.0042\mu_B$/f.u. for a magnetic field of $\mu_0 H \simeq 5$ T. The small moment together with the Brillouin shape ($M \sim \mathcal{B}_J(J, g, T, H)$) is characteristic of a few uncorrelated magnetic moments.

For an octrahedral coordination of the Rh^{3+} ion, the resulting crystal electric field (CEF) lifts the degeneracy of the five 4d orbitals and splits them into three lower and two higher energy levels, t_{2g} and e_g, respectively. If the Hund's coupling is smaller than the gap caused by the CEF spitting, the six remaining electrons in the 4d shell occupy the t_{2g} orbitals resulting in $S = L = 0$, a non-magnetic low-spin state. The small paramagnetic signal observed is characteristic of a fraction of magnetic impurities.

3 Conclusions

Using solid-state synthesis and chemical vapour transport, either larger quantities of phase-pure polycrystalline samples or high-quality single crystals of a 2D Janus material were synthesised. Single crystals grown by chemical vapor transport exhibit hexagonal and plate-like morphologies. The crystal structure of RhSeCl was successfully investigated using single crystal data and powder X-ray diffraction. The non-centro-

symmetric crystal structure consists of alternating layers of edge-linked Rh-octahedra, whereby the octahedral angle is distorted by the heteroleptic coordination. Magnetisation measurements reveal the diamagnetic nature of this compound. The synthesis *via* the CVT process is an excellent way to synthesise crystalline 2D Janus materials. As theoretical investigations predict the use of semiconducting RhTeCl[27] as a possible photo-catalyst for water splitting,[28] we expect the same for RhSeCl due to its structural similarities. Through exfoliation or nanocrystal growth it should be possible to further explore the phenomena of the 2D Janus material.

4 Materials and methods

4.1 Synthesis

All chemicals for the synthesis were used without further purification. $RhCl_3$ (rhodium(III) chloride, 99%, Abcr, lot 1251061) Rh (rhodium, 99.95%, Sigma-Aldrich, lot MKCQ0506), and Se (selenium, 99.999%, Alfa Aesar, lot S17G004) were used for the synthesis. All chemicals were handled inside an MBraun MB-200B ECO Glovebox at <1 ppm O_2 and <1 ppm H_2O. A stoichiometric ratio of 2 : 1 : 3 of rhodium, rhodium(III)-chloride and selenium was chosen in both cases for the synthesis of the polycrystalline powder samples and for crystal growth *via* chemical vapour transport (CVT). In case a larger quantity of RhSeCl is needed, we used solid-state synthesis and for single crystals we prefered CVT. The chemicals were mixed in an agate mortar and then transferred to a fused silica (imasil PN, qsil, max. 45 ppm OH content) single chamber ampoule. The ampoule was sealed with a hydrogen–oxygen torch under vacuum at 10^{-3} Pa.

For the solid-state synthesis, the samples were heated at a rate of 2 K min^{-1} at 950 °C for five days and then cooled to room temperature. A greyish powder was obtained. The CVT (see Fig. 6) was carried out with a temperature gradient of $\Delta T = 100$ K ($T_1 = 850$ °C, $T_2 = 950$ °C) at a heating rate of 2.5 K min^{-1}. After five days, the ampoule was allowed to naturally cool down to room temperature and small black, shiny crystals of RhSeCl were visible in the sink area. After opening the ampoules, isopropanol was added to the sink side and transferred to an ultrasonic bath and kept for 2 minutes to remove the crystals from the glass wall.
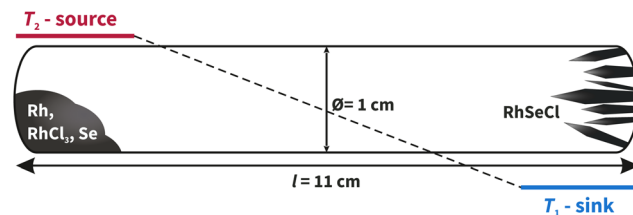

Fig. 6 Schematic diagram of the growth configuration for the performed experiments. One-chamber ampoules ($l = 11$ cm, $\varnothing = 1$ cm) were used, with the starting material positioned on the source side and the crystals deposited on the sink side.

2914 | *Inorg. Chem. Front.*, 2023, **10**, 2911–2916

This journal is © the Partner Organisations 2023

4.2 Identification and characterisation

Powder X-ray diffraction measurements were performed using a STADI P (STOE, Germany) device (Ge (111) primary beam monochromator, Mythen 1K detector, 0.015° step size) in transmission geometry with a Co source (λ = 1.78896 Å). For the Rietveld refinement, the Jana2006[29] program package was used. Single crystal X-ray diffraction was carried out using a BRUKER VENTURE8 with APEX3 software for data collection and integration. For the crystal structure solution, Jana2006[29] was used together with extitSUPERFLIP.[30] The crystals grown *via* CVT were investigated using light microscopy with the AXIO Imager.A1M (Fa. Zeiss, Germany). Therefore, we used the dark field image mode. SEM images were obtained using a Nova NanoSEM (Fa. FEI Company, USA) with a through-the-lens detector. The chosen accelerating voltage was varied within 15 keV. For the EDX analysis and mapping, we used a QUANTA 200/400 (Fa. AMETEX) with an accelerating voltage of 25 keV integrated into the SEM. Magnetic measurements of RhSeCl were performed in a VSM-SQUID magnetometer (MPMS, Quantum Design). The variation of magnetisation with temperature was recorded in field-cooled (FC) mode in the range from 300 K to 2 K and an applied field of 1 T.

Author contributions

D. N.: conceptualisation, methodology, investigation, visualisation, writing – original draft, writing – review & editing, and funding acquisition. M. V.: investigation, resources, writing – review & editing, and funding acquisition. B. R.: investigation, writing – original draft, and writing – review & editing. S. F. and S. E.: methodology and writing – review & editing. B. B.: resources and writing – review & editing. S. H.: project administration, funding acquisition, supervision, writing – original draft, and writing – review & editing. N. G.: project administration, supervision, writing – original draft, and writing – review & editing.

Conflicts of interest

The authors declare that they have no known competing financial interests or personal relationships that could have appeared to influence the work reported in this paper.

Acknowledgements

References

1 H. Kageyama, K. Hayashi, K. Maeda, J. P. Attfield, Z. Hiroi, J. M. Rondinelli and K. R. Poeppelmeier, Expanding frontiers in materials chemistry and physics with multiple anions, *Nat. Commun.*, 2018, **9**, 772.

2 G. Natta, P. Corradini and G. Allegra, The different crystalline modifications of $TiCl_3$, a catalyst component for the polymerization of α-olefins. I: α-, β-, γ-$TiCl_3$. II: δ-$TiCl_3$, *J. Polym. Sci.*, 1961, **51**, 399–410.

3 M. Grönke, U. S. F. Arrozi, N. Bronkalla, P. Schmidt, M. Valldor, S. Oswald, T. G. Woodcock, V. Eckert, Q. Hao, L. Plüschke, A. Lederer, K. Nielsch, B. Büchner, S. Kaskel and S. Hampel, Layered α-$TiCl_3$: Microsheets on YSZ Substrates for Ethylene Polymerization with Enhanced Activity, *Chem. Mater.*, 2019, **31**, 5305–5313.

4 Z. Yu, Z.-Y. Ong, S. Li, J.-B. Xu, G. Zhang, Y.-W. Zhang, Y. Shi and X. Wang, Analyzing the Carrier Mobility in Transition-Metal Dichalcogenide MoS_2 Field-Effect Transistors, *Adv. Funct. Mater.*, 2017, **27**, 1604093.

5 A. K. Singh, P. Kumar, D. Late, A. Kumar, S. Patel and J. Singh, 2D layered transition metal dichalcogenides (MoS_2): Synthesis, applications and theoretical aspects, *Appl. Mater. Today*, 2018, **13**, 242–270.

6 M. Valldor, Anion Ordering in Bichalcogenides, *Inorganics*, 2016, **4**, 23.

7 M. Yagmurcukardes, Y. Qin, S. Ozen, M. Sayyad, F. M. Peeters, S. Tongay and H. Sahin, Quantum properties and applications of 2D Janus crystals and their superlattices, *Appl. Phys. Rev.*, 2020, **7**, 011311.

8 D. B. Trivedi, G. Turgut, Y. Qin, M. Y. Sayyad, D. Hajra, M. Howell, L. Liu, S. Yang, N. H. Patoary, H. Li, M. M. Petrić, M. Meyer, M. Kremser, M. Barbone, G. Soavi, A. V. Stier, K. Müller, S. Yang, I. S. Esqueda, H. Zhuang, J. J. Finley and S. Tongay, Room-Temperature Synthesis of 2D Janus Crystals and their Heterostructures, *Adv. Mater.*, 2020, **32**, 2006320.

9 X. Tang and L. Kou, 2D Janus Transition Metal Dichalcogenides: Properties and Applications, *Phys. Status Solidi B*, 2022, **259**, 2100562.

10 C. Casagrande, P. Fabre, E. Raphaël and M. Veyssié, "Janus Beads": Realization and Behaviour at Water/Oil Interfaces, *Europhys. Lett.*, 1989, **9**, 251–255.

11 M. S. Bahramy and N. Ogawa, Bulk Rashba Semiconductors and Related Quantum Phenomena, *Adv. Mater.*, 2017, **29**, 1605911.

12 L. Zhang, Z. Yang, T. Gong, R. Pan, H. Wang, Z. Guo, H. Zhang and X. Fu, Recent advances in emerging Janus two-dimensional materials: from fundamental physics to device applications, *J. Mater. Chem. A*, 2020, **8**, 8813–8830.

13 S. W. Ng, N. Noor and Z. Zheng, Graphene-based two-dimensional Janus materials, *NPG Asia Mater.*, 2018, **10**, 217–237.

14 C. W. Jang, W. J. Lee, J. K. Kim, S. M. Park, S. Kim and S.-H. Choi, Growth of two-dimensional Janus MoSSe by a single in situ process without initial or follow-up treatments, *NPG Asia Mater.*, 2022, **14**, 15.

This journal is © the Partner Organisations 2023

Inorg. Chem. Front., 2023, **10**, 2911–2916 | **2915**

15 D. Hajra, R. Sailus, M. Blei, K. Yumigeta, Y. Shen and S. Tongay, Epitaxial Synthesis of Highly Oriented 2D Janus Rashba Semiconductor BiTeCl and BiTeBr Layers, *ACS Nano*, 2020, **14**, 15626–15632.

16 J. Kretschmer, PhD Thesis, Rheinischen Friedrich–Wilhelms–Universität Bonn, 2018.

17 J. Köhler and W. Urland, RhTeCl - das erste Chalkogenidhalogenid eines Platinmetalls mit Schichtstruktur, *Z. Anorg. Allg. Chem.*, 1997, **623**, 583–586.

18 M. Binnewies, R. Glaum, M. Schmidt and P. Schmidt, *Chemical Vapor Transport Reactions*, De Gruyter, 2012.

19 R. Mas-Ballesté, C. Gómez-Navarro, J. Gómez-Herrero and F. Zamora, 2D materials: to graphene and beyond, *Nanoscale*, 2011, **3**, 20–30.

20 H. Putz and K. Brandenburg GbR, *Diamond – Crystal and Molecular Structure Visualization*, 2022.

21 E. Parthé, E. Hohnke and F. Hulliger, A new structure type with octahedron pairs for Rh_2S_3, Rh_2Se_3 and Ir_2S_3, *Acta Crystallogr.*, 1967, **23**, 832–840.

22 H. Bärnighausen and B. Handa, Die Kristallstruktur von Rhodium(III)-chlorid, *J. Less-Common Met.*, 1964, **6**, 226–231.

23 T. Hahn, H. Klapper, U. Müller and M. I. Aroyo, *International Tables for Crystallography, Volume A*, 2016, pp. 720–776.

24 W. Borchardt-Ott, *Crystallography*, Springer Berlin Heidelberg, Berlin, Heidelberg, 2012.

25 W. Liu, K. T. Lai, K. Eckhardt, Y. Prots, U. Burkhardt and M. Valldor, Synthesis and characterization of sulfide oxide SrZnSO with strongly polar crystal structure, *J. Solid State Chem.*, 2017, **246**, 225–229.

26 J. You, S. Bongu, Q. Bao and N. Panoiu, Nonlinear optical properties and applications of 2D materials: theoretical and experimental aspects, *Nanophotonics*, 2018, **8**, 63–97.

27 H. Qu, S. Guo, W. Zhou, B. Cai, S. Zhang, Y. Huang, Z. Li, X. Chen and H. Zeng, Electronic structure and transport properties of 2D RhTeCl: A NEGF-DFT study, *Nanoscale*, 2019, **11**, 20461–20466.

28 Y. Ying, K. Fan, S. Zhu, X. Luo and H. Huang, Theoretical Investigation of Monolayer RhTeCl Semiconductors as Photocatalysts for Water Splitting, *J. Phys. Chem. C*, 2020, **124**, 639–646.

29 V. Petříček, M. Dušek and L. Palatinus, Crystallographic Computing System JANA2006: General features, *Z. Kristallogr. – Cryst. Mater.*, 2014, **229**, 345–352.

30 L. Palatinus and G. Chapuis, SUPERFLIP – a computer program for the solution of crystal structures by charge flipping in arbitrary dimensions, *J. Appl. Crystallogr.*, 2007, **40**, 786–790.

2916 | *Inorg. Chem. Front.*, 2023, **10**, 2911–2916

This journal is © the Partner Organisations 2023